Investigation of the causes of historical changes in the sub-surface salinity minimum of the South Atlantic

Marlos Goes,[1] Ilana Wainer,[2], and Natalia Signorelli[2]

Corresponding author: Marlos Goes, CIMAS/University of Miami and NOAA/AOML, Miami, USA. (marlos.goes@noaa.gov)

[1]CIMAS/University of Miami and NOAA/AOML, Miami, USA.

[2]Institute of Oceanography, University of São Paulo,São Paulo, Brazil

Abstract.

In this study we investigate the sub-surface salinity changes on decadal timescales across the Subtropical South Atlantic Ocean using two ocean reanalysis products, the latest version of the Simple Ocean Data Assimilation and the Estimating the Circulation and Climate of the Ocean, Phase II , as well as with additional climate model experiments. Results show that there is a recent significant salinity increase at intermediate levels. The main underlying mechanism for this sub-surface salinity increase is the lateral advective (gyre) changes due to the Southern Annular mode variability, which conditions an increased contribution from the Indian Ocean high salinity waters. The global warming signal has a secondary but complementary contribution. Latitudinal differences at intermediate depth in response to large-scale features are in part caused by local variation of westward propagation features, and by compensating contributions of salinity and temperature to density changes.

1. Introduction

Modulation and stability of the South Atlantic meridional overturning circulation are dependent on salinity changes [*Weijer et al.*, 2002; *Peeters et al.*, 2004], and an improved understanding of the mechanisms behind these salinity variations, especially the signature of change below the ocean surface, is essential for better monitoring and prediction of long-term climate change.

Long-term changes in ocean salinity are a function of large scale atmospheric forcing as well as regional freshwater fluxes. In the South Atlantic Ocean significant ocean warming, driving trends in freshwater fluxes, has been documented from observations and is the subject of much research [*Gille*, 2002; *Curry et al.*, 2003; *Boyer et al.*, 2005; *Grodsky et al.*, 2006; *Boning et al.*, 2008; *Schmidtko and Johnson*, 2012; *McCarthy et al.*, 2012]. Ocean salinity changes are in general depth and latitudinally dependent [*Curry et al.*, 2003]. They are larger in the top 500 m of the ocean because of the direct effect of atmospheric fluxes. In comparison to earlier data on record (1960–1970s), more recent years (1990s) have shown salinity increases in the tropical-subtropical latitudes due to warming and increased evaporation [*Boyer et al.*, 2005], and salinity decreases in the extratropical regions due to increased precipitation and runoff (including ice melting).

However, these long-term changes are subject to intense interannual and decadal variability [*Grodsky et al.*, 2006], and more recent data show an actual decrease in surface salinity in the tropical Atlantic due to increased precipitation and upwelling. This impacts the mixed layer depth, and therefore the formation of subsurface water masses. Water masses that are formed on the base of the mixed layer are in contact with the atmosphere for a relative short period during their formation. They are eventually subducted into the ocean interior following mostly an adiabatic pathway along neutral density surfaces. At depth they are also modified by mixing which acts on much longer timescales. Below the surface, the signature of salinity changes in the ocean is subject to higher uncertainty than at the surface, since salinity is dynamically entangled with the temperature field, which together determine the density [*Pierce et al.*, 2012]. Therefore, understanding salinity changes in the South Atlantic at intermediate depths requires understanding the relative contribution of the associated processes [*Durack and Wijffels*, 2010], such as surface atmospheric forcing, circulation changes, changes due to mixing along the water-mass pathways, and vertical movements of isopycnals due to wind field effects. In the South Atlantic, an important wind effect can be related to changes in the Southern Annular Mode (SAM) through variations in sea level pressure (SLP), which in turn would impact on the surface wind leading to a broad-scale surface warming associated with the poleward migration of isopycnal outcrops [*Durack and Wijffels*, 2010; *Schmidtko and Johnson*, 2012].

Although frequent in situ salinity data are scarce in the South Atlantic before 2002, several studies have used historical ship-based conductivity– temperature–depth (CTD) along with more recent Argo floats data to investigate long-term changes in the Sub-Antarctic Mode Water (SAMW) and in the Antarctic Intermediate Water (AAIW) salinity minimum layer underneath. Their results indicate cooling and freshening of the SAMW, and warming and salinification associated with the AAIW [*Bindoff and McDougall*, 1994; *Boning et al.*, 2008; *McCarthy et al.*, 2011; *Schmidtko and Johnson*, 2012], in addition to a statistically significant strong circumpolar AAIW isopycnals shoaling, accompanying a decrease in density, and an equatorward spreading of the salinity anomalies at the sub-surface [*Durack and Wijffels*, 2010; *Schmidtko and Johnson*, 2012]. A further decrease in the AAIW density is also projected for the 21st century in climate models [*Goes et al.*, 2008].

Further analysis of Argo observations reveals the variability of the AAIW salinity in the South Atlantic on interannual and intradecadal timescales. Westward propagating salinity anomalies at 30°S show that Rossby wave mechanisms are important for the interpretation of salinity changes associated with the hydrological cycle of the AAIW at these timescales [*McCarthy et al.*, 2012].

In this study we investigate changes in the sub-surface salinity minimum of the South Atlantic and its relation to large-scale trends such as those related to global warming via greenhouse gases and the Southern Annular Mode (SAM). For this we use a blend of ocean reanalyses and process oriented climate model experiments. This paper is outlined as follows: Section 2 describes the two ocean reanalyses used in this study; Section 3 shows the results of the examination of the two reanalysis data, followed by the analysis of the climate model experiments. The setup of the climate model experiments is presented in an Appendix; Sections 4 and 5 contain a discussion of the results and the conclusion of this study.

2. Data

The first part of this study utilizes temperature and salinity data from the Simple Ocean Data Assimilation (SODA) version 2.2.6 [*Ray and Giese*, 2012], and from the Estimating the Circulation and Climate of the Ocean, Phase II (ECCO2). They can be described as follows:

2.1. SODA 2.2.6

SODA 2.2.6 uses the Parallel Ocean Program (POP) model [*Smith et al.*, 1992] at a 1/4° horizontal resolution, which is publicly available at an interpolated 0.5° x 0.5° horizontal resolution, and 40 vertical levels at monthly averages, spanning the period of 1871 to 2008. Vertical diffusion of momentum, heat, and salt are carried out using K-profile parameterization (KPP) mixing with modifications to address issues such as diurnal heating, while lateral subgrid-scale processes are modeled using biharmonic mixing.

Surface boundary conditions used are from eight ensemble members of the NOAA atmospheric Twentieth Century reanalysis 20Crv2 [*Compo et al.*, 2011]. SODA 2.26 assimilates only sea surface temperature (SST) data using a sequential estimation data assimilation method [*Carton and Giese*, 2008]. The SST data comes from the ICOADS 2.5 SST product (http://icoads.noaa.gov), which is based purelly on in-situ observations (e.g., XBT, CTD, bottle, Argo) and reached 2 million data report per year in 1960s. Heat and salt fluxes in SODA are calculated from bulk formulae using 20CRv2 daily variables. By not assimilating in-depth hydrography and only SST, the model is more dinamically consistent over different decades than alternative versions. A complete overview of the ocean-reanalysis process is detailed by *Carton and Giese* [2008].

2.2. ECCO2

The Estimating the Circulation and Climate of the Ocean, Phase II (ECCO2) project [textitMenemenlis, 2008] An ECCO2 data synthesis is obtained by least-squares fit of a global full-depth-ocean and sea-ice configuration of the Massachusetts Institute of Technology OGCM (Marshall et al. 1997) to the available satellite and in situ data. This least-squares fit is carried out for a small number of control parameters using a Green's function approach [textitMenemenlis, 2005]. The solution requires the computation of a number of sensitivity experiments that are free, unconstrained calculations by a forward model. The experiments are designed to adjust the model parameters, forcing, and initial conditions. Then the model is run forward again using the adjusted parameters, free of any constraints, as in any ordinary model simulation. The model employs a cube-sphere grid projection with a mean horizontal grid spacing of 18 km and 50 vertical levels. Surface forcings such as wind and precipitation are from the JRA25 reanalysis [*Onogi*, 2007].

3. Results

3.1. AAIW properties in SODA and ECCO2

As stated in the previous section, SODA 2.2.6 assimilates only SST data. This allows the model to be more dynamically consistent over time, although larger differences may exist with respect to actual hydrographic data. Salinity data in the South Atlantic are historically sparse, mostly available in a more consistent way since the 2000s from Argo floats measurements. ECCO2 uses a Green functions method, which also allows a smooth salinity path over time, and allows a stronger hydrographic constraint with depth. We estimate the differences in the representation of the AAIW in both reanalyses by comparing their salinity properties with an Argo climatology [*Roemmich and Gilson*, 2009], which is available at a 1 degree horizontal resolution starting in 2004, for a similar period. The Argo climatology exhibits a minimum salinity tongue in the central basin (at 25 °W; Figure 1c) extending from its formation region (between 45 and 60°S) across the mixed layer to a maximum depth of 600–1200 m at 35-40°S. The salinity minimum follows closely the depth of the isopycnal σ_θ =27.2 Kg/m^3, which is approximately 1000 m deep in this region. Previous studies have associated the depth of the salinity minimum with the σ_θ =27.2 Kg/m^3 isopycnal surface, and also with the neutral density surface γ_n =27.4 Kg/m^3 [*You*, 2002]. North of 20 °S, the σ_θ =27.2 Kg/m^3 density surface levels out to a depth of 700 m, and the salinity minimum flows underneath a salty surface region of maximum evaporation minus precipitation (E-P).

SODA shows features analogous to the observations over a similar period (i.e., 2004–2009; Figure 1a). In SODA, the isopycnals south of 40°S are much more inclined than observations, and the maximum depth of the σ_θ =27.2 Kg/m^3 is approximately 1200 m deep, 200 m deeper than the observations. The salinity minimum in the South Atlantic is also deeper in SODA than in the observations. This causes a maximum anomaly of salinity on 40°S of up to 0.6 psu at 500 m depth (Figure 1d). At ~7°S, SODA shows a strong near-surface upwelling region, characterized by an uplifting of the isopycnals. This feature is not evident in the ARGO climatology. ECCO2 shows a more consistent structure than SODA, the minimum salinity is well constrained at approximately 800 m, and the differences os salinity with depth are therefore much reduced ($<$ 02 psu) in comparison to SODA (Figure 1e).

Next, we compare the regional features of the salinity minimum in the South Atlantic between the reanalyses and Argo, doing so after interpolating all products to the Argo resolution. The salinity minimum surface in the South Atlantic is shown in Figure 2. SODA shows a stronger Subantarctic Front (STF; $\sim$ 45 °S) than in observations (Figure 2a, c), which agrees with the larger isopycnal slopes in that region, as revealed in Figure 1a. For this reason the STF region shows the largest salinity differences ($\sim$ 0.3) between SODA and Argo (Figure 2d). In the other regions salinity differences are smaller, and can reach approximately 0.1 in magnitude. ECCO2 (Figure 2b) shows an improvement in the STF region in comparison to SODA, and the biases are below 0.15 psu in the region. North of 30°S, biases in ECCO2 and SODA show similar magnitudes. Although there are differences between the two reanalysis products and observations, their similarities, and specially the dissimilarities with respect to the model assimilation schemes they are based on, show that their temporal and spatial variability, once they agree between the products, must be robust with respect to the variability of the AAIW in the region.

3.2. Regional trends in the AAIW

In the South Atlantic, changes in the relationship of temperature and salinity along isopycnals show latitudinal dependence. The time and latitude distribution of the South Atlantic salinity at various density levels from the 1960s to 2000s is here inferred from Temperature-Salinity (θ/S) diagrams for four latitudes (35°S, 30°S, 20°S, 10°S; Figure 3).

At 35°S (Figure 3a), there is an increase in salinity in the latter years in the thermocline waters. This increase is not monotonic over time, instead alternating, with the 1970s and 1990s having lower salinity values, and the 1960s, 1980s and 2000s having higher salintiy values. Similar alternating patterns are found along 30°S and 10°S (Figures 3b and 3d, respectively). At 10°S, which is located in the tropical region of high E-P, salinity increases by 0.2 in the upper tropical waters, which is related to an increase in the hydrological cycle in the region [*Curry et al.*, 2003; *Helm et al.*, 2010]. At 20°S (Figure 3c), the 2000s have lower salinity values at the thermocline, and higher values in the 1970s. The smallest differences in θ/S over time are achieved at 20°S in the whole profile. The central and intermediate water levels generally have opposing signs of changes at all latitudes. Central waters show a recent cooling and freshening along isopycnals, as is apparent in the density layer between $\sigma = 26.5$ and 27.0 kg m^{-3}, whereas intermediate waters generally show warming and increased salinity between $\sigma = 27.2$ and 27.4 kg m^{-3} (highlighted in the insets of Figure 3).

To investigate the time variability of the ocean properties at the salinity minimum position, we produce a time series of the salinity, potential density (σ_θ) and temperature anomalies relative to the average over the whole time series period at the depth of the salinity minimum, for two locations in the central part of the basin, at 25°W/30°S and 25°W/35°S (Figure 4). At both latitudes, there is an increase in salinity and temperature in the late 1980s/beginning of 1990s until the end of the series (Figure 4a,c,d,f). This joint effect of warming and salinification produces a reduction in density during this period (Figure 4b,e); a feature that agrees with climate projections of the AAIW [*Goes et al.*, 2008]. The effect of the density decrease at the minimum salinity depth is more prominent at 35°S than at 30°S. There is strong decadal variability at both latitudes, although fluctuations appear in different periods: at 30°S, there is a general freshening trend from the 1960s to the 1970s, and an increase in salinity after 1976. The rate of salinity increase from the mid-1970s to the mid-1990s is the highest with about 0.01 per decade, while it levels out considerably in the late 1990s and 2000s. At 35°S there is a significant positive salinity anomaly in the 1970s, followed by an also significant negative salinity anomaly in the 1980s. A linear trend of about 0.05 per decade is apparent after that. Trends observed after 2000 in all analyzed parameters exceed 3 standard deviations (red dashed lines in Figure 4) calculated for the whole time series period, showing that these trends are likely to be statistically significant.

These interannual-to-decadal salinity changes are consistent with recent findings that changes in the rate of global surface temperature increase have occurred in previous decades, such as in the mid-1970s [*Levinson and Lawrimore*, 2008; *Trenberth and Coauthors*, 2007], and that these changes can potentially produce signals in density and salinity at depth [*Durack and Wijffels*, 2010].

3.3. Density changes in the subtropical Atlantic

According to *Bindoff and McDougall* [1994], salinity changes at depth have three main causes: i) freshening/salinification on isopycnals, ii) warming/cooling on isopycnals and iii) heave, which is related to vertical displacements of isopycnals without changes in salinity and temperature. Therefore, knowledge of these salinity changes requires understanding the causes of density changes at intermediate levels.

We investigate the causes of variability of density around the salinity minimum depth ($\sim$ 1140 m) by estimating the thermopycnal and halopycnal changes at that depth. For this we keep the salinity or temperature constant at their climatological means, and let the other component vary over time. This way, we are able to estimate the main contribution of density changes, which drive the large-scale meridional water displacement in the ocean.

We calculate the temperature and salinity contributions to density changes for the latitudes of 30° and 35°S at 25°W (Figure 5). At 30°S, SODA shows an increase in potential density from $\sim$ 27.29 kg m^{-3} in the 1960s to $\sim$ 27.32 kg m^{-3} in the 1970s. A subsequent increase in potential density at 1140 m is manifested after 1985 and continues until 2008, where it assumes a value of $\sim$ 27.28 kg m^{-3}. These potential density changes are driven mostly by temperature changes (red line) at this latitude. At 35°S (Figure 5b), there is a similar increase in potential density in the 1970s and a decrease afterwards. Interestingly, the total density behavior does not closely follow the changes driven only by temperature. Instead, there is a strong compensation between temperature and salinity at 35°S. This behavior can explain the larger variability of salinity values on isopycnals at 35°S than at 30°S, shown in Figure 4.

3.4. Subtropical Gyre variability

An AAIW layer, which encompasses the the salinity minimum surface depths ($\sim$ 800–1100 m), is constructed by defining two neutral density surfaces as the upper and lower boundaries, the $\gamma_n = 27.1$ and $\gamma_n = 27.6$, respectively. Within this layer, there is a signature of the inflow of salty Indian Ocean waters through the southeastern tip of the Atlantic. The high salinity Indian Ocean waters at intermediate levels are formed in the Red Sea [*Talley*, 2002]. After entering the South Atlantic, these waters lose their signature through mixing along their trajectory westward. A minimum on the salinity minimum surface is obvious at about 30°S (Figure 6a), crossing the basin from east to west following the Benguela Current Extension [*Schmid and Garzoli*, 2009], which feeds into the Brazil Current (BC) along the western boundary. BC waters encounter the Malvinas Current waters between 35°S and 40°S, resulting in a westward inflow of low salinity waters along the South Atlantic Current.

SODA shows decadal changes in salinity between the 1960 and 2000 (Figure 6b–e). Compared to the 1960s, the 1970s and 1980s show a slight decrease in the minimum salinity in most parts of the South Atlantic. A noticeable feature in the 1970s and later on in the 1990s and 2000s is the southward shift of the Brazil-Malvinas confluence up to about 3 degrees, in comparison to the 1960s. The 1980s, in opposition, shows a northward migration of the confluence, which can explain some of the decadal variability shown in Figures 4). The 1990s show reduced salinity in the center of the salinity minimum south of 35°S, and a general increase of salinity in the rest of the basin. Of great importance is the increased inflow of higher salinity waters from the Agulhas Current retroflection region in the southeastern part of the basin, which increases the signature of these waters toward the northwestern part of the basin. In the 2000s, this trend of increasing salinity in the basin continues, and increased salinity values are found also on the western side of the basin. This can have implications for the interhemispheric transport through the North Brazil Undercurrent.

Advective mechanisms within the gyre have potential to drive a large part of the salinity increase displayed in SODA. This can be quantified by potential vorticity (PV) maps for the defined intermediate layer (Figure 7). The Ertel's PV is calculated as:

$$PV = \frac{f}{\rho_0}\frac{\Delta\gamma_n}{\Delta z} \qquad (1)$$

where f is the Coriolis parameter, ρ_0 is the mean density of the ocean, and Δz is the layer thickness. It is clear from the PV maps (Figure 7) that the PV has become more negative inside the subtropical gyre at the AAIW layer, which characterizes a spin-up of the anticyclonic gyre recently. Additionally, there has been an expansion of the gyre southward, in agreement with observational results of the surface subtropical gyre [*Roemmich et al.*, 2007; *Goni et al.*, 2011], and poleward migration of the ACC [*Gille*, 2008]. This would preclude waters flowing from the Drake Passage and ACC from entering the southern boundary of the South Atlantic, and would also reduce the mixing between the Agulhas and SAC waters, making higher salinity waters prevail in the gyre.

3.5. Westward propagating Rossby Waves

As noted by *McCarthy et al.* [2012], salinity anomalies can be generated at intermediate depths in the eastern side of the basin, and propagate westward with a second mode Rossby wave speed. *McCarthy et al.* [2012] suggests that this can be an important mechanism to explain the variability of the salinity minimum across the basin on interannual timescales. In Figure 6, there is a clear extension of the subtropical gyre and increase in the Agulhas leakage at intermediate depths. The Agulhas leakage is well correlated with the strength of the westerlies [*Durgadoo et al.*, 2013] in the eastern part of the Atlantic basin. Similarly to *Durgadoo et al.* [2013], we define an index for the strength of the westerlies in the eastern part of the basin as the average zonal wind stress within 35°S–65°S and 0°W–20°E.

To investigate how salinity anomalies originated in the Agulhas leakage region and forced by the westerly winds spread over the South Atlantic, we apply a lagged correlation of the westerly wind stress index in the eastern side of the basin to the salinity minimum surface. The time series are previously smoothed with a 9-month Boxcar window to filter the seasonal variability. The maximum lagged correlations and their lags are shown in Figure 8. The lag of the maximum correlation over space shows the propagation patterns of the salinity anomalies. Small lag values, close to zero or even negative, are observed in the eastern side of the basin. Negative lag values in the southeastern tip of the basin show that the flow in the Agulhas leakage is driven in great part by the wind stress anomalies east of Africa. Where the lag shows smaller values, the correlation of the westerlies and the salinity anomalies is highest, above 0.6. Anomalies propagate along a northwestern trajectory, following the ocean circulation at that depth (Figure 7). This is also characteristic pattern of a Rossby wave signal, which phase speed decreases poleward. A larger extension of anomalies propagation is revealed along 29°S. South of 30°S the lag increases considerably up to 200 months, i.e., about 17 years.

To investigate whether Rossby wave propagation is a plausible dynamical mechanism for the variability of the AAIW on interannual to decadal timescales, we produced time-longitude plots (Hovmoller diagrams) at two latitudes, 30°S and 35°S (Figure 9). Hovmoller diagrams allow us to determine zonal propagation patterns along a given latitude. In these diagrams, propagating waves appear as diagonal bands across the basin, and the slopes of these patterns are equal to the phase speed (c_p) of the waves. Here, wave characteristics are assessed objectively using the Radon Transform (RT) applied to the Hovmoller diagrams [*Challenor et al.*, 2001; *Polito and Liu*, 2003; *Barron et al.*, 2009]. This method rotates the coordinate system of the zonal-temporal diagrams in order to find the patterns that best align with the rotated axis.

The Hovmoller diagrams are for salinity anomalies (calculated with respect to the annual mean climatology) projected onto the γ_n=27.4 neutral surface. Zonal means are subtracted from the anomalies field to filter decadal trends [*Barron et al.*, 2009], thus highlighting the interannual timescales. West-to-east propagating anomalies spread along 30°S. The optimal propagation speed is cp = 1.79 ± 0.48 cm s^{-1}, at which anomalies travel across the basin in approximately 10 years. A similar result is obtained in the lag correlation maps shown in Figure 8. These speeds strongly agree with those obtained by *McCarthy et al.* [2012], who estimated a propagation speed of cp = 1.7 cm s^{-1}, which is characteristic of a second baroclinic mode wave propagation. At 35°S, the situation is different. Propagation speeds of 0.47 ± 0.06 cm s^{-1} are much slower than the one predicted by the Rossby wave theory. In fact, the pattern of the variability in the eastern part of the basin (east of 15°W) seems to be unrelated to the one further west. From the lag correlation maps, we observe that the correlations decrease considerably from east to west at this latitude, and therefore mixing and advective mechanisms must play a larger role in the regional dynamics.

3.6. Wind x CO_2

In the previous sections we show that SODA 2.2.6 exhibits changes in the subsurface salinity minimum and circulation patterns at intermediate layers. These changes include decadal variability overlapping a background low frequency variability, which becomes stronger after the 1970s. Other studies confirm that similar subsurface changes have ocurred since 1950 [e.g., *Levitus et al.*, 2000; *Gille*, 2002; *Levitus et al.*, 2005; *Domingues et al.*, 2008; *Levitus et al.*, 2009; *Durack and Wijffels*, 2010; *Gille*, 2008; *Lyman et al.*, 2010].

In order to examine the possible causes of the salinity minimum variability, we perform idealized experiments with an Earth System Model of Intermediate Complexity in which two possible forcings, the wind stress curl changes in the Atlantic and the global warming due to CO_2 are separated. In these experiments, we use the University of Victoria Earth System Model of Intermediate Complexity (UVic 2.9) [*Weaver et al.*, 2001]. This model has been widely used in climate simulations and model comparison studies. We separate the influences of the wind stress on the advective mechanisms in the South Atlantic into northern and southern hemispheric forcings, by defining the first hemispheric modes of variability, which are related to the North Atlantic Oscillation (NAO) and SAM, to the north and south respectively. A description of the model experiments can be found in Appendix A.

3.6.1. AAIW changes in the intermediate complexity model

Similarly to Figure 4, we show the time series of salinity and temperature at the location of the salinity minimum at 30°S and 25°W (Figure 10). For each index, four time series are shown, which represent the index calculated for the experiments described in Appendix A. The CONTROL simulation, without transient forcing (red curve), shows a salinity of ~ 34.57 and temperature of ~ 4.39 °C from 1870 to 2009. Salinity changes, relative to the CONTROL simulation, driven by wind changes in response to atmospheric pressure changes due to the SAM (green curve in Figure 10a) are negative from 1870 to 1950 in the model. Changes in the SAM phase after the 1960s drive positive salinity anomalies, modulated by decadal variability. In 2008, the salinity is 0.015 above the pre-industrial level. When a NAO-like forcing is considered in addition to the SAM forcing (blue curve in Figure 10), additional changes are minor, and the trends due to wind variability in the model resemble strongly the SAM-only experiment. Finally, when CO_2 forcing is added on the top of SAM and NAO forcings (turquoise curve in Figure 10), there is an increased positive trend in AAIW salinity after 1950 in comparison to the SAM-only experiment. This trend driven by the CO_2 load in the atmosphere is strongly linear, and the 2008 salinity anomaly relative to the pre-industrial values is 0.025. Therefore, the CO_2 forcing on AAIW salinity anomalies is responsible for 50% of the changes due to SAM in the 2000s. Although secondary in driving historical salinity anomalies in the AAIW, CO_2 forcing is the main contributor for the increase in temperature anomalies at the depth of the salinity minimum (Figure 10b). While SAM-like forcing accounts for 0.1°C relative to the CONTROL run, adding the CO_2 forcing increases the temperature anomalies to 0.3°C, a contribution of 2/3 of the recent warming of the AAIW, while SAM accounts for just 1/3. NAO-like forcing is again a minor contribution to the AAIW variability in the South Atlantic.

Salinity minimum changes in UVic are heterogeneous over the spatial domain (Figure 11). This feature agrees with those features manifested in SODA (Figure 6). Here we separate the recent (2000s) effects of the considered external forcings on the salinity minimum by subtracting hierarchically a simulation with that forcing from another simulation without it.

Adding SAM as a forcing mechanism produces salinity anomalies with a dipole pattern (Figure 11b), in which there is a salinity increase north of 35°S and mostly a decrease south of 35°S. Anomalies generated by an NAO-like pattern (Figure 11c) are much reduced with respect to the SAM or CO_2 forcings, and show mostly negative salinity anomalies within the subtropical gyre. Forcing due to increased CO_2 concentration in the 2000s produce a salinity increase in the subtropical South Atlantic, and negative anomalies along the South Atlantic Current. The CO_2 response is similar but weaker than the response forced by SAM, although south of 45°S the CO_2 response exhibits an increased salinity on the northern edge of the ACC.

4. Discussion

Many physical processes can cause changes in the South Atlantic variability in particular, and in the Southern Hemisphere climate in general. These range from greenhouse gases concentrations in the atmosphere (CO_2), to the major modes of coupled variability. These atmospheric patterns can cause non-monotonic interdecadal fluctuations in the θ/S relationships at depth, as revealed in previous studies [e.g., *Garabato et al.*, 2009]. SODA and the climate model experiments performed here show that the largest changes in the salinity minimum are associated with changes in the gyre, and with trends in SAM, which in turn will impact water mass formation processes through its relationship with the associated surface winds. NAO variability largely affects Labrador Sea and Greenland Sea water formation, which in turn affects water properties in the North Atlantic, especially the North Atlantic Deep Water [*Arbic and Brechner Owens*, 2001]. According to our results, air-sea climate modes in the North Atlantic do not seem to affect the spread of the salinity minimum in the South Atlantic. The positive trend in SAM is associated with cooling at high southern latitudes and strengthening of the latitudinal temperature gradient, leading to stronger subtropical and westerly winds [*Hall and Visbeck*, 2002; *Silvestri and Vera*, 2003; *Lefebvre et al.*, 2004; *Sen Gupta and England*, 2006; *Gillett et al.*, 2006; *Toggweiler et al.*, 2009; *Thompson et al.*, 2011]. The reader is referred to *Thompson et al.* [2011] for an extensive review. In addition, *Durgadoo et al.* [2013] show from a hierarchy of models that an equatorward (poleward) shift in westerlies increases (decreases) the Agulhas leakage. This occurs because of the redistribution of momentum input by the winds. It is concluded that the reported present-day leakage increase could therefore reflect an unadjusted oceanic response mainly to the strengthening westerlies over the last few decades. *Bindoff and McDougall* [1994] analyze salinity and temperature changes in isopycnals as pure heating, pure freshening and heave. More recent studies call attention to the lateral advection of these properties along isopycnals, and therefore, circulation changes would be a source of salinity changes on isopycnals [*Durack and Wijffels*, 2010]. Here we confirm the role of lateral advection in reducing the low salinity waters from the Drake Passage due to the Atlantic subtropical gyre expansion, as well as increasing leakage of salty Agulhas waters at intermediate levels.

5. Conclusions

By investigating the decadal changes in the minimum salinity layer for the subtropical South Atlantic we have established the relationship between density changes with large scale climate trends. Significant trends are observed in SODA since the late 1990s in salinity, temperature and density at intermediate levels. We found a latitudinal dependence on the contribution of temperature and salinity to density changes that would ultimately drive the meridional water displacement in the ocean. South of 35°S there is strong compensation between salinity and temperature, which may drive larger trends in those fields because of the dynamical influence of salinity. North of 35°S, temperature is by far the largest driver of density changes.

In SODA we determined two main dynamic factors for the salinity increase in the South Atlantic salinity minimum region: i) the expansion and spinup of the subtropical gyre reduces the influx of the low salinity waters from the Pacific, which follow a path through the Drake Passage into the South Atlantic; and ii) the strengthening of the westerlies forces an increase in the Agulhas leakage, and, therefore, the input of high salinity waters at intermediate depths into the South Atlantic. Different dynamic mechanisms are also present at different latitudes which determine the spread of the high salinity waters from the southeast boundary into the Atlantic. At 30°S, the anomalies generated by the westerlies in the southeastern Atlantic follow a path defined by the Benguela Current and the Benguela Current Extension, in which changes in salinity at this latitude are highly driven by ocean adjustment through a second mode Rossby wave mechanism. This result is in agreement with previous studies [e.g., *McCarthy et al.*, 2012]. At 35°S, mixing is the main mechanism to carry anomalies from the east, since propagation times are much larger than what linear wave theory suggests, and the correlation with the eastern source of anomalies is decreased.

The sensitivity studies with the UVic2.9 model indicate that the SAM is the predominant forcing of salinity changes in the sub-surface South Atlantic when compared to the NAO and GHG forcing. GHG was shown to represent 50% of the changes due to SAM, and therefore about 1/3 of the total magnitude of the salinity changes of the AAIW, although GHG produces most of the temperature changes in the AAIW level.

Appendix A: The climate model of intermediate complexity

In the present work we use the latest version of the University of Victoria Earth System Model (UVic 2.9). The ocean component of UVic 2.9 [*Weaver et al.*, 2001] is MOM2 [*Pacanowski*, 1995] with a 1.8° x 3.6° resolution in the horizontal and 19 depth levels. Diapycnal diffusivity is parameterized as $K_v = K_{tidal} + K_{bg}$, which consists of the mixing due to local dissipation of tidal energy (K_{tidal}) [*Laurent et al.*, 2002; *Simmons et al.*, 2004] plus a background diffusivity $K_{bg} = 0.3$ cm^2 s^{-1}. The atmospheric component is a one-layer atmospheric energy-moisture balance model, which does not apply flux correction and is forced by prescribed winds from the NCEP/NCAR climatology. Also included in the model are a thermodynamic sea ice component, a terrestrial vegetation (TRIFFID), and an oceanic biogeochemistry based on the ecosystem model of [*Schmittner*, 2005]. The model is spun up for 3000 years, and then four experiments are performed (Table 1). First, the CONTROL experiment is a non-transient experiment forced with atmospheric forcings from the 1800 levels. The second to fourth experiments use, in addition to the NCEP/NCAR wind stress climatology, wind stress anomalies calculated from the first empirical mode (EOF1) of sea level pressure (SLP) anomalies in the northen and southern hemispheres (Figure 12). These modes are a good approximation of the North Atlantic Oscillation (NAO), in which the positive phase is characterized by low SLP anomalies over Iceland and high SLP anomalies over the Azores, and the Southern Annular Mode (SAM), which is characterized by low SLP anomalies over Antarctica, respectively. More specifically, the second experiment uses the SAM EOF forcing only, the third experiment uses the NAO EOF forcing only, and the fourth experiment uses both the SAM and the NAO forcings plus historical global CO_2 emissions, under which the atmospheric CO_2 concentration levels reach 384 ppmV in 2009. The hemispheric SLP modes are calculated from the *Compo et al.* [2006] dataset and start in the year 1871. When the SLP anomalies related to the hemispheric modes of variability are added to the model, the associated wind stress anomalies are calculated using a frictional geostrophic approximation [*Weaver et al.*, 2001]. This wind stress is also converted to wind speed for the calculation of the latent and sensible heat fluxes from the ocean [*Fanning and Weaver*, 1998]. All experiments are run from 1800–2008, keeping the other atmospheric forcings (e.g., sulphate and volcanic aerosols) at the 1800 level.

Acknowledgments. This work is supported in part by NOAA/AOML and NOAA's Climate Program Office, and by grants from CAPES-ciencias-do-mar, 2013/02111-4 of the São Paulo Research Foundation (FAPESP),CNPq-300223/93-5 and CNPq-MCT-INCT-Criosfera 573720/2008-8.

References

Arbic, B. K., and W. Brechner Owens (2001), Climatic Warming of Atlantic Intermediate Waters*, *J. Climate*, *14*, 4091–4108.

Barron, C. N., A. B. Kara, and G. A. Jacobs (2009), Objective estimates of westward rossby wave and eddy propagation from sea surface height analyses, *J. Geophys. Res.*, *114*, C03,013.

Bindoff, N. L., and T. J. McDougall (1994), Diagnosing climate change and ocean ventilation using hydrographic data, *J. Phys. Oceanogr*, *24*, 1137–1152.

Boning, C. W., A. Dispert, S. M. Visbeck, R. Rintoul, and F. U. Schwarzkopf (2008), The response of the Antarctic Circumpolar Current to recent climate change, *Nature Geosci.*, *1*, 864–869.

Boyer, T., S. Levitus, J. Antonov, R. Locarnini, and H. Garcia (2005), Linear trends in salinity for the world ocean, 1955–1998, *Geophys. Res. Lett*, *32*(1), 1–4.

Carton, J., and B. Giese (2008), A reanalysis of ocean climate using simple ocean data assimilation (SODA), *Mon. Weath. Rev.*, *136*(8), 2999–3017.

Challenor, P. G., P. Cipollini, and D. Cromwell (2001), Use of the 3D radon transform to examine the properties of oceanic Rossby waves, *J. Atmos. Oceanic Technol.*, *18*, 1558–1566.

Compo, G., J. Whitaker, and P. Sardeshmukh (2006), Feasibility of a 100-year reanalysis using only surface pressure data, *Bull. Amer. Meteor. Soc.*, *87*, 175–190.

Compo, G., J. Whitaker, P. Sardeshmukh, N. Matsui, R. Allan, X. Yin, B. Gleason, R. Vose, G. Rutledge, P. Bessemoulin, et al. (2011), The twentieth century reanalysis project, *Quart. Jour. Royal Met. Soc.*, *137*(654), 1–28.

Curry, R., B. Dickson, I. Yashayaev, et al. (2003), A change in the freshwater balance of the atlantic ocean over the past four decades, *Nature*, *426*(6968), 826–829.

Domingues, C. M., J. A. Church, N. J. White, P. J. Gleckler, S. E. Wijffels, P. M. Barker, and J. R. Dunn (2008), Improved estimates of upper-ocean warming and multi-decadal sea-level rise, *Nature*, *453*(7198), 1090–1093.

Durack, P., and S. Wijffels (2010), Fifty-year trends in global ocean salinities and their relationship to broad-scale warming, *J. Climate*, *23*(16), 4342–4362.

Durgadoo, J. V., B. R. Loveday, C. J. C. Reason, P. Penven, and A. Biastoch (2013), Agulhas leakage predominantly responds to the Southern Hemisphere westerlies, *J. Phys. Oceanogr.*, *43*, 21132131.

Fanning, A. F., and A. J. Weaver (1998), Thermohaline variability: The effects of horizontal resolution and diffusion, *J. Climate*, *11*(4), 709–715.

Garabato, A. C. N., L. Jullion, D. P. Stevens, K. J. Heywood, and B. A. King (2009), Variability of subantarctic mode water and antarctic intermediate water in the drake passage during the late-twentieth and early-twenty-first centuries, *J. Climate*, *22*(13), 3661–3688.

Gille, S. (2008), Decadal-scale temperature trends in the Southern Hemisphere ocean, *J. Climate*, *21*, 4749–4765.

Gille, S. T. (2002), Warming of the southern ocean since the 1950s, *Science*, *295*, 1275–1277.

Gillett, N., T. Kell, and P. Jones (2006), Regional climate impacts of the Southern Annular Mode, *Geophys. Res. Lett.*, *33*(23).

Goes, M., I. Wainer, P. R. Gent, and F. O. Bryan (2008), Changes in subduction in the South Atlantic Ocean during the 21st century in the CCSM3, *Geophys. Res. Lett.*, *35*, 6701–+.

Goni, G. J., F. Bringas, and P. N. DiNezio (2011), Observed low frequency variability of the Brazil Current front, *J. Geophys. Res. – Oceans*, *116*(C10037).

Grodsky, S., J. Carton, and F. Bingham (2006), Low frequency variation of sea surface salinity in the tropical Atlantic, *Geophys. Res. Lett.*, *33*(14), L14,604.

Hall, A., and M. Visbeck (2002), Synchronous variability in the Southern Hemisphere atmosphere, sea ice, and ocean resulting from the annular mode*, *J. Climate*, *15*(21), 3043–3057.

Helm, K. P.,N. L. Bindoff, andJ. A. Church (2010), Changes in the global hydrological-cycle inferred from ocean salinity,textitGeophys. Res. Lett.,*37*, L18701.

Laurent, L. S., H. Simmons, and S. Jayne (2002), Estimating tidally driven mixing in the deep ocean, *Geophys. Res. Lett.*, *29*(23), 2106.

Lefebvre, W., H. Goosse, R. Timmermann, and T. Fichefet (2004), Influence of the Southern Annular Mode on the sea ice–ocean system, *J. Geophys. Res.: Oceans*, *109*(C9).

Levinson, D. H., and J. H. Lawrimore (2008), State of the climate in 2007, *Bull. Amer. Meteor. Soc.*, *89*, S1–S179.

Levitus, S., J. Antonov, T. Boyer, and C. Stephens (2000), Warming of the world ocean, *Science*, *287*, 2225–2229.

Levitus, S., J. I. Antonov, and T. P. Boyer (2005), Warming of the world ocean, 1955-2003, *Geophys. Res. Lett.*, *32*, L02,604.

Levitus, S., J. Antonov, T. Boyer, R. Locarnini, H. Garcia, and A. Mishonov (2009), Global ocean heat content 1955–2008 in light of recently revealed instrumentation problems, *Geophys. Res. Lett.*, *36*(7).

Lyman, J. M., S. A. Good, V. V. Gouretski, M. Ishii, G. C. Johnson, M. D. Palmer, D. M. Smith, and J. K. Willis (2010), Robust warming of the global upper ocean, *Nature*, *465*(7296), 334–337.

McCarthy, G., E. McDonagh, and B. King (2011), Decadal Variability of Thermocline and Intermediate Waters at 24°S in the South Atlantic, *J. Phys. Oceanogr.*, *41*, 157–165.

McCarthy, G. D., B. A. King, P. Cipollini, E. L. McDonagh, J. R. Blundell, and A. Biastoch (2012), On the sub-decadal variability of South Atlantic Antarctic Intermediate Water, *Geophys. Res. Lett*, *39*, L10,605.

D. Menemenlis, I. Fukumori, and T. Lee (2005), Using Green's functions to calibrate an ocean general circulation model. *Mon. Weather Rev.*, *133*, 1224–1240.

D. Menemenlis, J. Campin, P. Heimbach, C. Hill, T. Lee, A. Nguyen, M. Schodlok, and H. Zhang (2008), ECCO2: High resolution global ocean and sea ice data synthesis. *Mercator Ocean Quarterly Newsletter*, *31*, 13–21.

Onogi, K., J. Tsutsui, H. Koide, M. Sakamoto, S. Kobayashi, H. Hatsushika, T. Matsumoto, N. Yamazaki, H. Kamahori, K. Takahashi, S. Kadokura, K. Wada, K. Kato, R. Oyama, T. Ose, N. Mannoji, and R. Taira (2007), The JRA-25 Reanalysis, *J. Meteor. Soc. Japan*, *85*, 369–432.

Pacanowski, R. (1995), MOM 2 documentation user's guide and reference manual, GFDL Ocean Group Technical Report No.3, *Fluid Dyn. Lab. NOAA, Princeton, NJ.*

Weijer, W., W. P. M. de Ruijter, A. Sterl, and S. S. Drijfhout (2002), Response of the Atlantic overturning circulation to South Atlantic sources of buoyancy, *Global Planet. Change*, *34*, 293–311.

Peeters, F. J. C., R. Acheson, G.-J. A. Brummer, W. P. M. de Ruijter, G. M. Ganssen, R. R. Schneider, E. Ufkes, and D. Kroon (2004), Vigorous exchange between Indian and Atlantic Ocean at the end of the last five glacial periods, *Nature*, *430*, 661–665.

Pierce, D. W., P. J. Gleckler, T. P. Barnett, B. D. Santer, and P. J. Durack (2012), The fingerprint of human-induced changes in the oceans salinity and temperature fields, *Geophys. Res. Lett.*, *39*, L21,704.

Polito, P. S., and W. T. Liu (2003), Global characterization of Rossby waves at several spectral bands, *J. Geophys. Res.*, *108*(doi:10.1029/2000JC000607).

Ray, S., and B. S. Giese (2012), Historical changes in El Niño and La Niña characteristics in an ocean reanalysis, *J. Geophys. Res.*, *117*, C11,007.

Roemmich, D., and J. Gilson (2009), The 2004-2008 mean and annual cycle of temperature, salinity, and steric height in the global ocean from the Argo program, *Progr. Oceanogr.*, *82*, 81–100.

Roemmich, D., J. Gilson, R. Davis, P. Sutton, S. Wijffels, and S. Riser (2007), Decadal spinup of the South Pacific subtropical gyre, *J. Phys. Oceanogr.*, *37*, 162–173.

Schmid, C., and S. L. Garzoli (2009), New observations of the spreading and variability of the Antarctic Intermediate Water in the Atlantic, *J. Marine Res.*, *67*(6), 815–843.

Schmidtko, S., and G. Johnson (2012), Multidecadal warming and shoaling of Antarctic Intermediate Water*, *J. Climate*, *25*, 207–221.

Schmittner, A. (2005), Decline of the marine ecosystem caused by a reduction in the Atlantic overturning circulation, *Nature*, *434*(7033), 628–633.

Sen Gupta, A., and M. H. England (2006), Coupled ocean-atmosphere-ice response to variations in the Southern Annular Mode, *J. Climate*, *19*(18), 4457–4486.

Silvestri, G. E., and C. S. Vera (2003), Antarctic oscillation signal on precipitation anomalies over southeastern South America, *Geophys. Res. Lett.*, *30*(21), 2115.

Simmons, H. L., S. R. Jayne, L. C. S. Laurent, and A. J. Weaver (2004), Tidally driven mixing in a numerical model of the ocean general circulation, *Ocean Modell.*, *6*(3), 245–263.

Smith, R., J. Dukowicz, and R. Malone (1992), Parallel ocean general circulation modeling, *Physica D: Nonlinear Phenomena*, *60*(1), 38–61.

Talley, L. D. (2002), *Salinity patterns*, 11 pages pp., Encyclopedia of Global Environmental Change, vol. 1, M. C. MacCracken and J. S. Perry, editors, John Wiley and Sons.

Thompson, D. W., S. Solomon, P. J. Kushner, M. H. England, K. M. Grise, and D. J. Karoly (2011), Signatures of the Antarctic ozone hole in Southern Hemisphere surface climate change, *Nature Geosc.*, *4*(11), 741–749.

Toggweiler, J., et al. (2009), Shifting westerlies, *Science*, *323*(5920), 1434–1435.

Trenberth, K. E., and Coauthors (2007), *Observations: Surface and atmospheric climate change*, 235–336 pp., S. Solomon et al., Eds., Cambridge University Press.

Weaver, A. J., M. Eby, E. C. Wiebe, C. M. Bitz, P. B. Duffy, T. L. Ewen, A. F. Fanning, M. M. Holland, A. MacFadyen, H. D. Matthews, et al. (2001), The UVic Earth system climate model: Model description, climatology, and applications to past, present and future climates, *Atmos.-Oc.*, *39*(4), 361–428.

You, Y. (2002), Quantitative estimate of Antarctic Intermediate Water contributions from the Drake Passage and the southwest Indian Ocean to the South Atlantic, *J. Geophys. Res.*, *107*, 3031.

Table 1. Summary of the climate model experiments.

Experiment	**Wind Forcing**	CO_2 **Forcing**
CONTROL	NCEP climatology	1800 level
SAM	NCEP clim plus SAM	1800 level
SAM + NAO	NCEP clim plus SAM plus NAO	1800 level
SAM + NAO + CO_2	NCEP clim plus SAM plus NAO	Transient to 384 ppmV in 2009

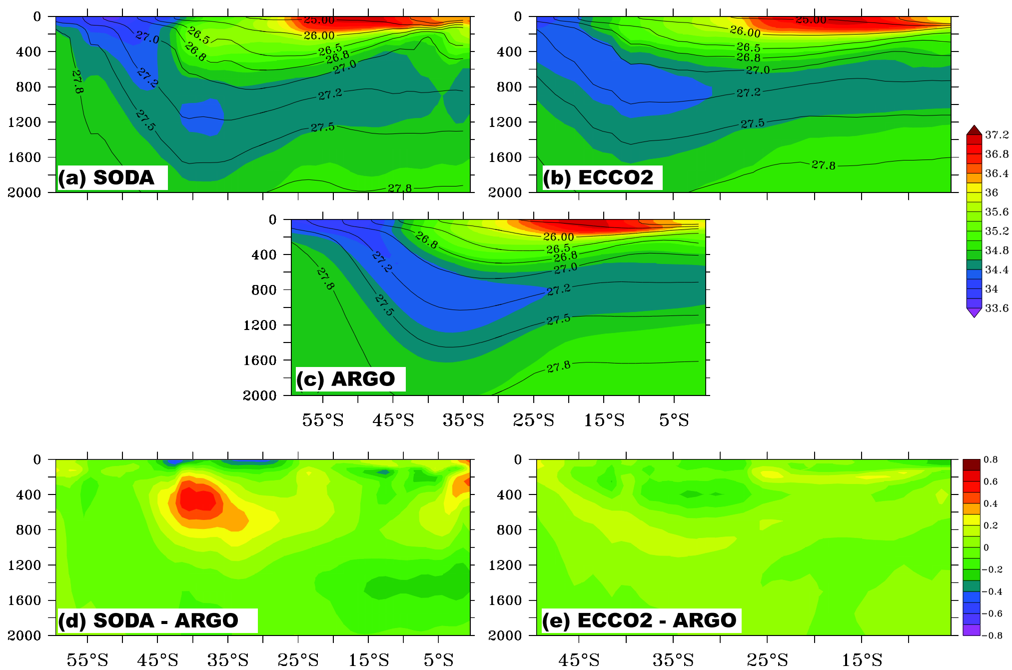

Figure 1. Meridional section of the climatological average (after 2004) of salinity at 25°W in the South Atlantic. Depth is in meters. Relevant potential density surfaces (σ_θ in Kg/m^3) are overlaid. Panel a) is for SODA, b) for ECCO2, c) for Argo climatology [*Roemmich and Gilson*, 2009], d) SODA - Argo and e) ECCO2 - Argo.

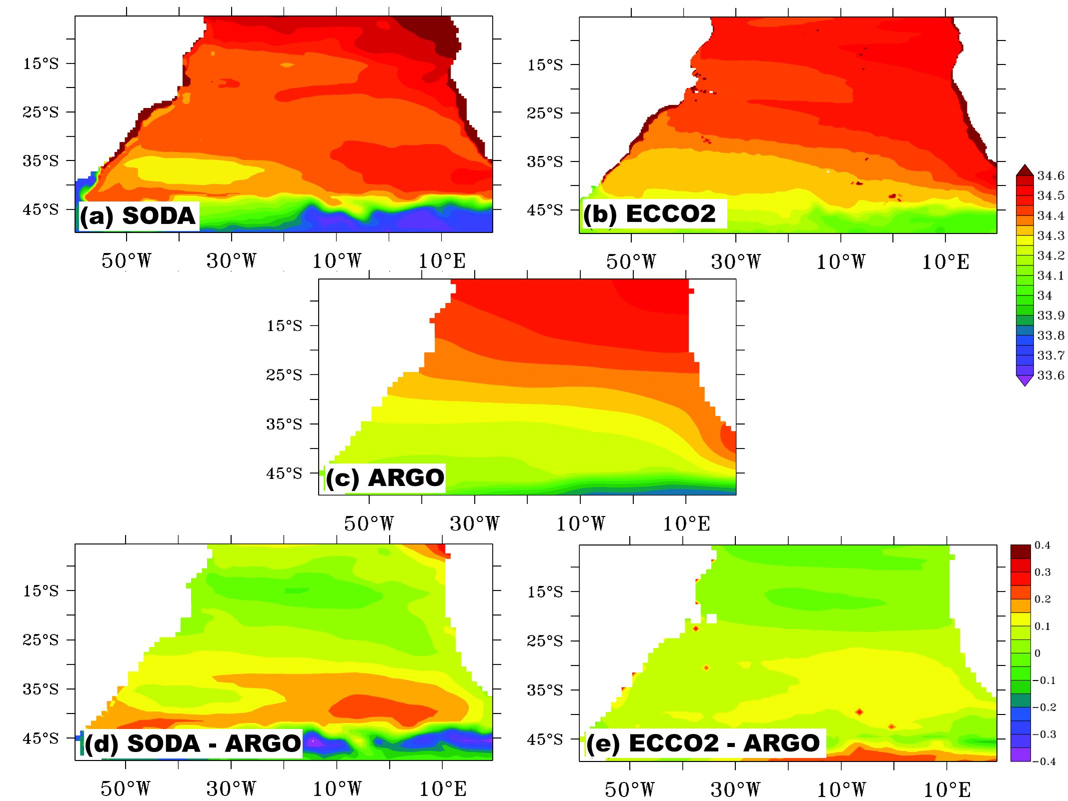

Figure 2. Maps of the climatological average (after 2004) of the salinity minimum surface in the South Atlantic. Panel a) is for SODA, b) for ECCO2, c) for Argo climatology [*Roemmich and Gilson*, 2009], d) SODA - Argo and e) ECCO2 - Argo.

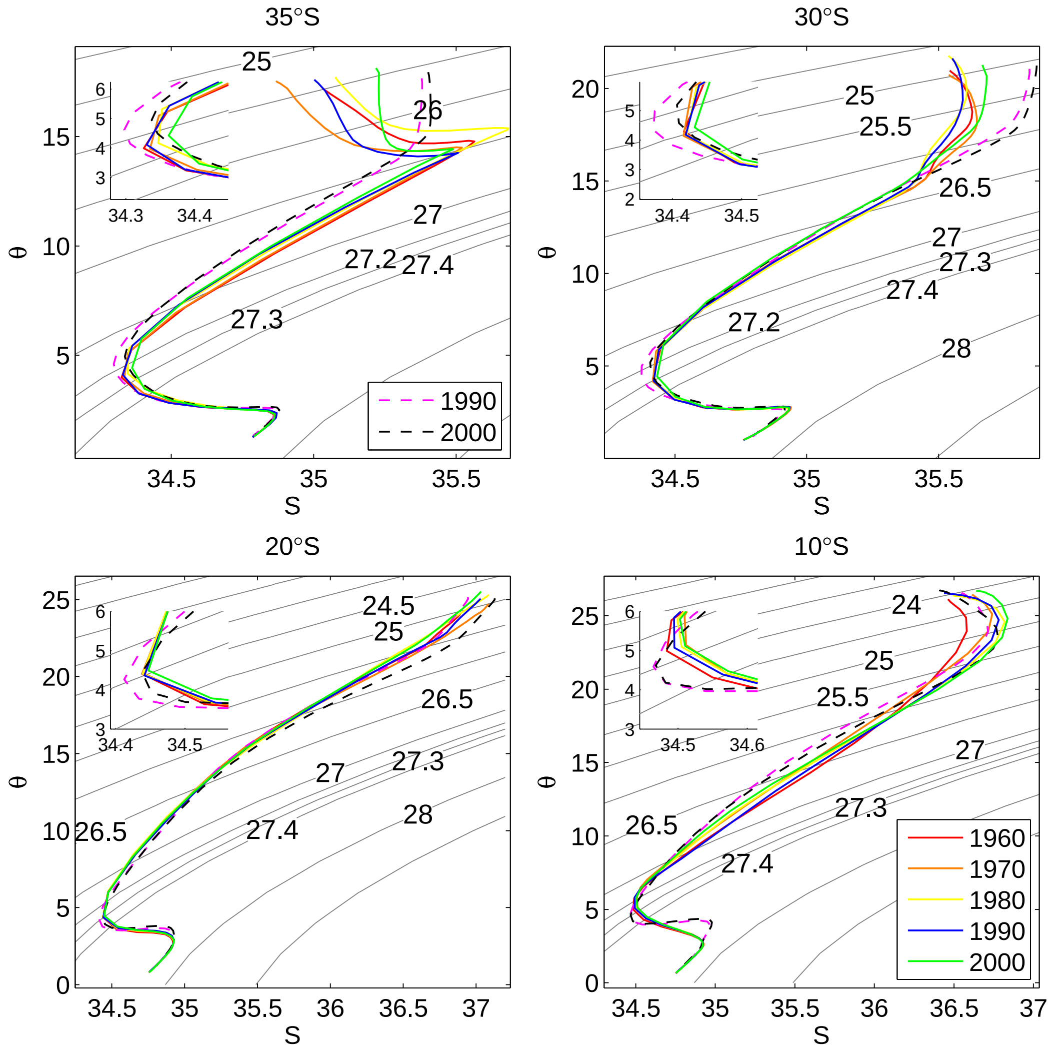

Figure 3. Θ/S diagram for the South Atlantic Ocean at 25°W for a) 35°S, b) 30°S, c) 20°S and d) 10°S. Solid colored lines represent SODA's decadal averages for the 1960s (red), 1970s (orange), 1980s (yellow), 1990s (green) and 2000s (blue). Dashed colored lines represent ECCO2's decadal averages for 1990s (magenta) and 2000s (black).

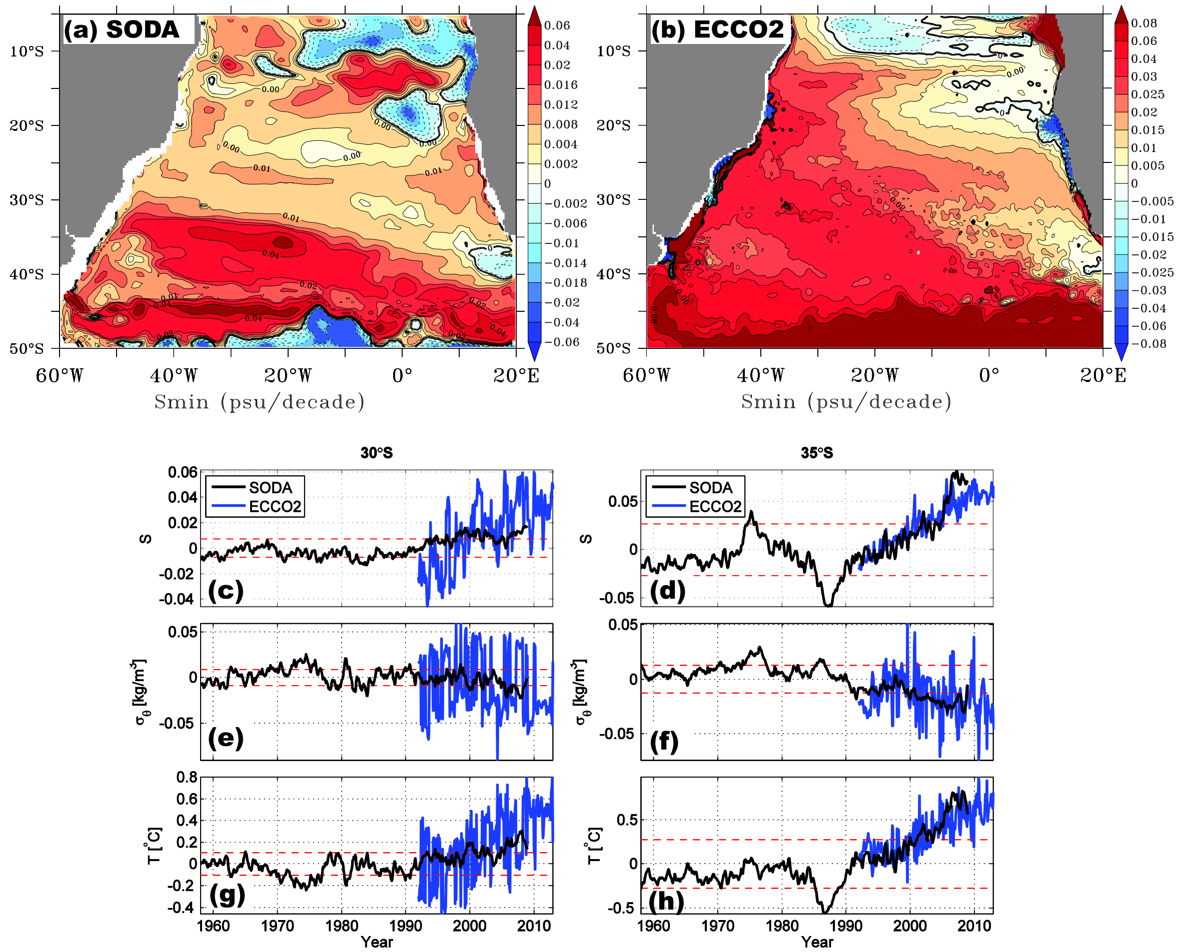

Figure 4. Salinity minimum trend between 1990's and 2000's (psu/decade) for (a) SODA and (b) ECCO2. Panels (c-h) are the time series of the salinity (c, d), sigma density (e,f), and temperature (g,h) anomalies with respect to SODA's 1960-2008 period at the location of the salinity minimum. Timeseries on the left column are for 25°W/30°S and on the right column for 25°W/35°S. Black timeseries is for SODA and blue is for ECCO2. The red dashed lines represent SODA's the three standard deviation levels relative to each parameter.

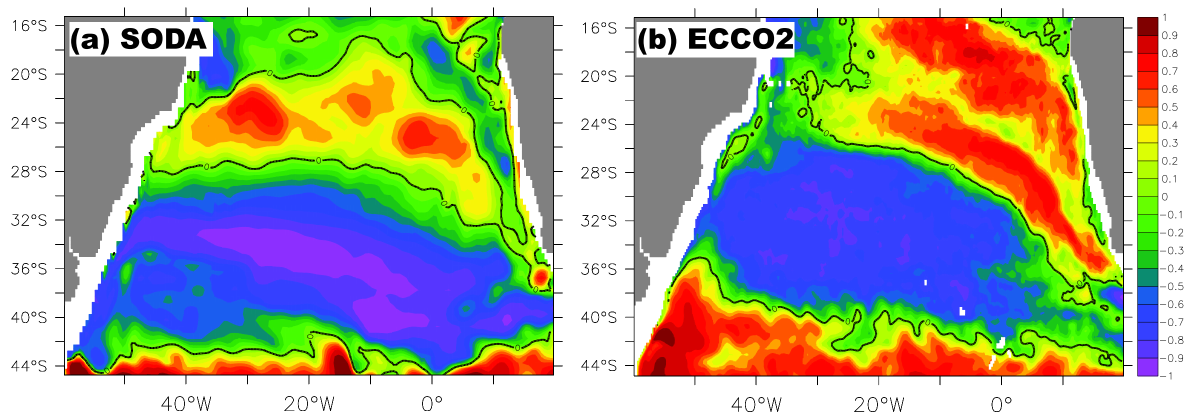

Figure 5. Correlation between the components of the sigma density, i.e., thermopycnal and halopycnal components, at approximately 1100 m depth for (a) SODA and (b) ECCO2. The components of sigma are calculated by keeping the other component as the climatological value.

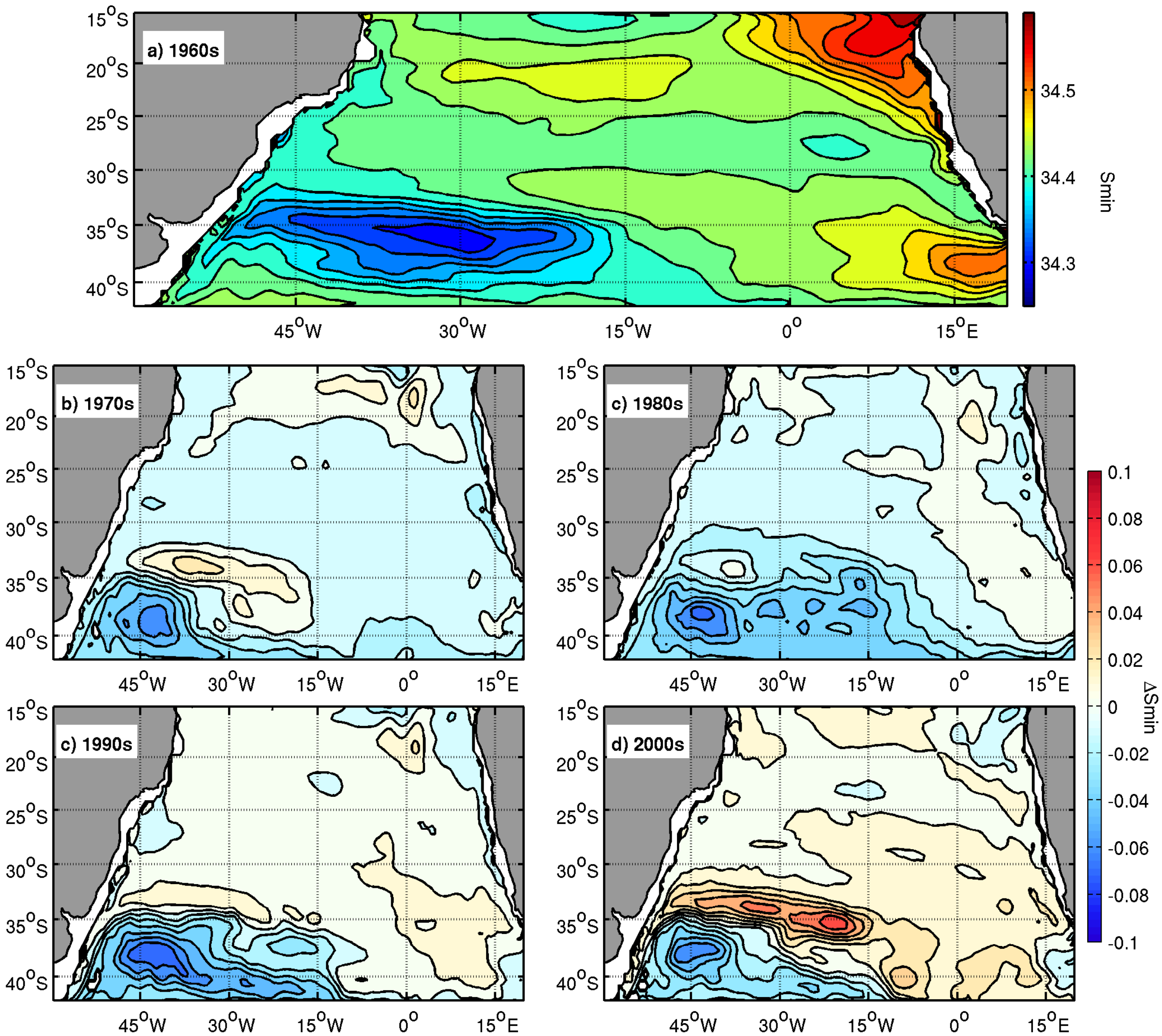

Figure 6. Salinity minimum within the layer defined by the $\gamma_n = 27.1$ and $\gamma_n = 27.6$ neutral surfaces for a) 1960s, b) 1970s, c) 1990s and d) 2000s.

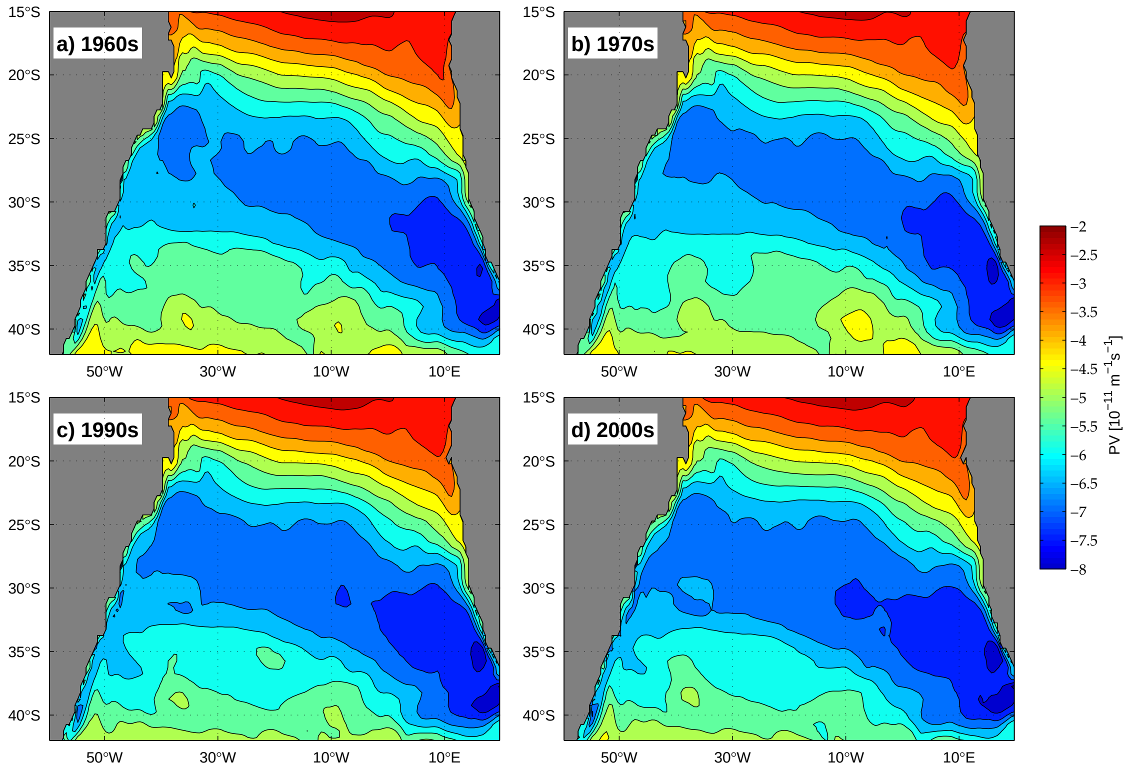

Figure 7. Ertel's potential vorticity calculated within the layer defined by the $\gamma = 27.1$ and $\gamma = 27.6$ neutral surfaces for a) 1960s, b) 1970s, c) 1990s and d) 2000s.

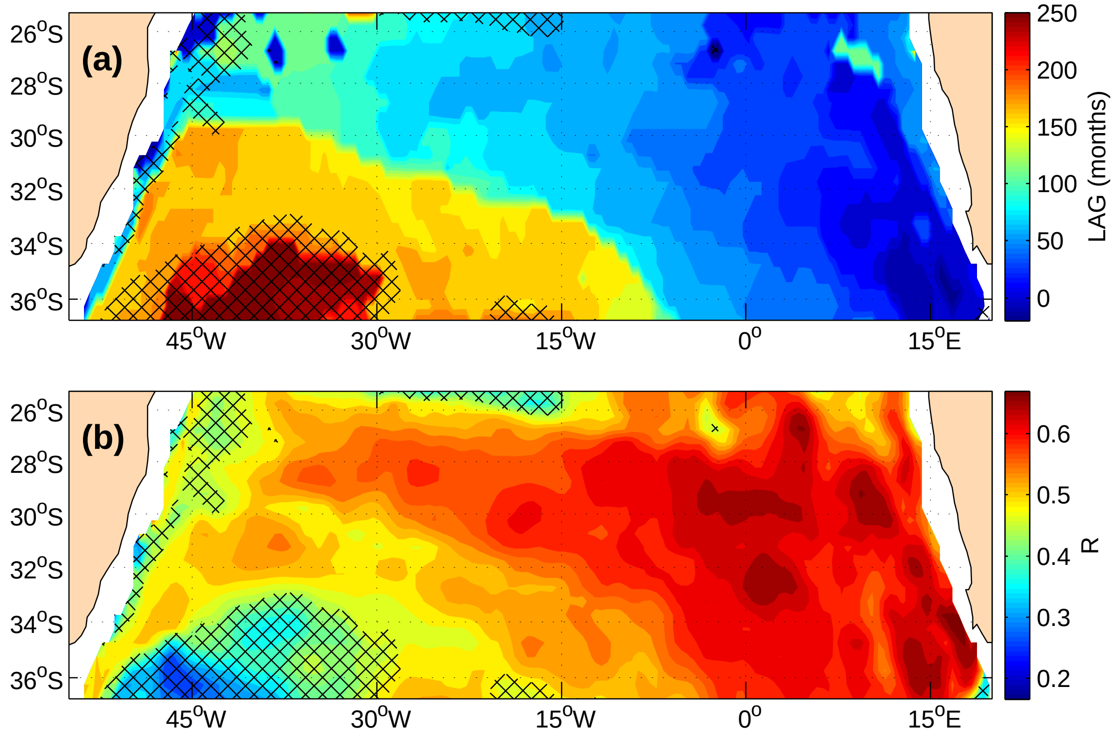

Figure 8. Maximum lagged correlation between the salinity at $\sigma_\theta = 27.2$ and a westerly wind strength index in the southeastern Atlantic, defined by the τ_x averaged between 35°S–65°S/0°E–20°E. (a) is the lag of the maximum correlation (months) and (b) is the maximum correlation. The crossed areas are where correlation values of the pre-whitened timeseries are not statistically significant.

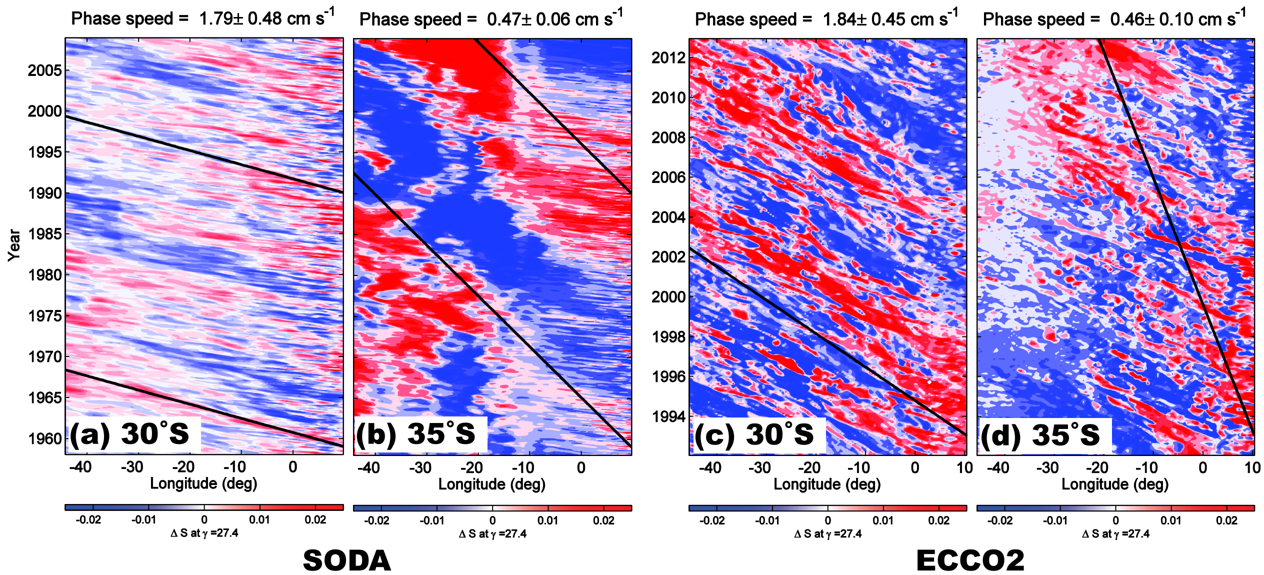

Figure 9. Time x Longitude diagram for the salinity anomalies projected onto the neutral density surface $\gamma_n = 27.4$, that defines the region of minimum salinity in the subtropical Atlantic at (a,c) 30°S and (b,d) 35°S. Panels (a,b) are for SODA and (c,d) are for ECCO2. Following *Barron et al.* [2009], the zonal average of the salinity anomalies is subtracted from the diagrams to highlight the propagating features. The phase speed calculated from the method of *Barron et al.* [2009] is shown on the top of each panel and its displacement is shown as a black line overlaid on the contours.

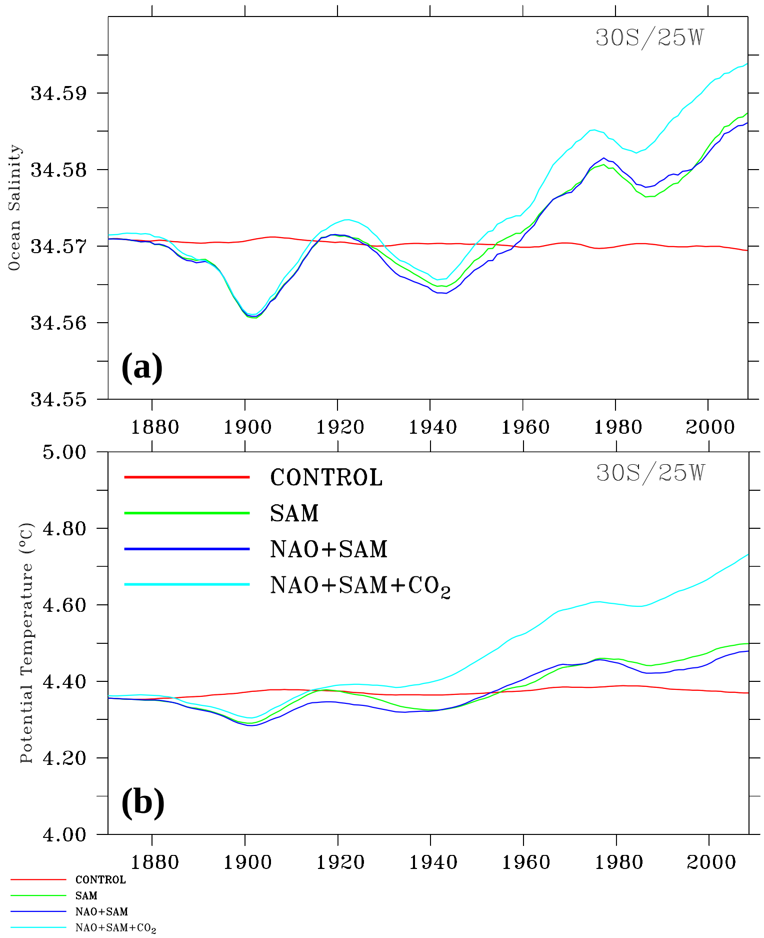

Figure 10. Time series of (a) salinity and (b) potential temperature at the salinity minimum depth at 30°S/25°W from the UVIC model experiments. The colored lines are for the CONTROL (red), SAM only (green), SAM plus NAO (dark blue), and NAO plus SAM plus CO_2 (cyan) experiments.

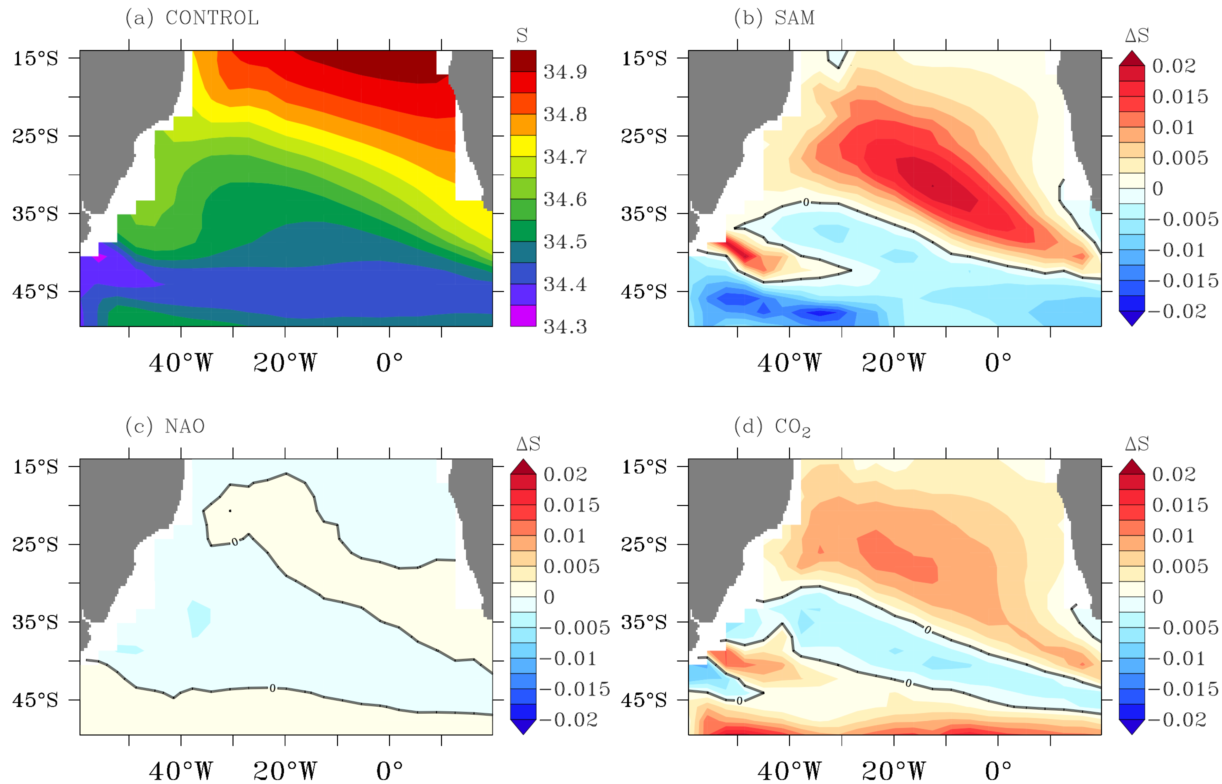

Figure 11. (a) South Atlantic salinity minimum in the Uvic CONTROL experiment averaged between 2000–2009. (b–d) Average (2000-2009) salinity minimum differences among the experiments, in which each panel shows how adding one forcing changes the salinity in comparison to the experiment without that forcing, for (b) SAM, (c) NAO, and (d) CO_2.

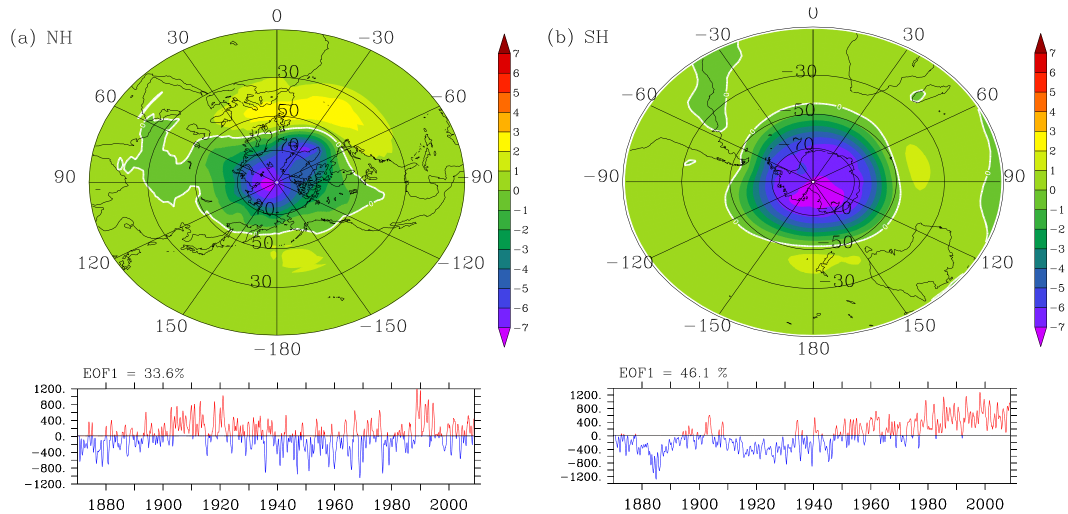

Figure 12. First EOF of the hemispheric sea level pressure used to force the atmospheric model in UVic for the (a) Northern Hemisphere and (b) Southern Hemisphere.